nature communications

Article

https://doi.org/10.1038/s41467-025-67271-w

Robust fast-switching black electrochromic windows based on solution-processed n-doped transparent organic conductor

Received: 12 July 2025

Accepted: 26 November 2025

Won-June Lee[1], Palak Mehra[1], Jonathan R. Thurston[2], Yanpei Tian[3], Xiaojie Liu[1,3], Sanket Samal[1], Liyan You[1], Inho Song[1,4], Xiulin Ruan[3], Michael F. Toney[5] & Jianguo Mei[1] ✉

Electrochromic (EC) windows face trade-offs in cost, switching speed, color neutrality, and durability. We present solution-processed n-doped poly(benzodifurandione) (n-PBDF) as a robust organic conductor for black EC windows overcoming these limitations. Utilizing an engineered solvent ink and ultrasonic spray coating, we achieve uniform large-area n-PBDF deposition under ambient conditions without additives. n-PBDF EC electrodes show unprecedented weathering durability (maintaining performance under simultaneous exposure to light (including UV), heat, and humidity for >768 h), addressing a key barrier for organic EC materials. The electrodes exhibit deep black coloration with color neutrality, rapid switching (<2 s), and remarkable cycling stability (>20,000 cycles). Large-area EC devices demonstrate uniform switching performance, confirming scalable fabrication. Building energy simulations of the EC window reveal significant HVAC savings potential across diverse transitional climates. This work establishes n-PBDF as a scalable, high-performance alternative to conventional inorganic EC systems, advancing the viability of solution-processable smart windows for sustainable architecture.

Electrochromic (EC) smart windows[1–4], which dynamically adjust light transmission in response to electrical stimuli, have emerged as promising energy-efficient solutions for modern buildings and vehicles. Early progress in *inorganic* EC materials—such as tungsten oxide-based systems commercialized by companies like Sage and View—brought these technologies to market over two decades ago[3]. However, their widespread adoption remains limited by persistent drawbacks: high production costs, slow switching speeds (seconds to minutes), and an inability to achieve a spectrally neutral gray state, which is essential for architectural aesthetics and glare reduction. Notably, recent reports have demonstrated that these limitations are being largely addressed in inorganic EC materials, as strategies including nanostructure control, ion doping, and electrolyte optimization have achieved enhanced switching performance and high optical modulations[5]. To overcome these limitations in processability and offer a broader functional scope, recent research has shifted toward *organic* EC materials, such as EC polymers. These materials enable low-cost, large-area manufacturing via roll-to-roll (R2R) solution processing, as demonstrated by companies like Ambilight in applications such as automotive sunroofs and side windows. Despite their cost and scalability advantages, organic EC systems face unresolved challenges in long-term durability, particularly under prolonged exposure to ultraviolet (UV) radiation, temperature cycling, and humidity—conditions critical for architectural applications requiring 20–30-year lifespans. The durability-performance gap is especially acute for black organic EC windows, which are uniquely valuable for energy-efficient solar control and

---

[1]James Tarpo Jr. and Margaret Tarpo Department of Chemistry, Purdue University, West Lafayette, IN, USA. [2]Department of Chemistry, University of Colorado, Boulder, CO, USA. [3]School of Mechanical Engineering, Purdue University, West Lafayette, IN, USA. [4]Department of Chemical Engineering, Chung-Ang University, Seoul, Republic of Korea. [5]Department of Chemical and Biological Engineering, Materials Science and Engineering Program, Renewable and Sustainable Energy Institute, University of Colorado, Boulder, CO, USA. ✉e-mail: jgmei@purdue.edu

visual privacy. Despite growing demand, commercially viable black EC windows with high durability, fast switching, and uniform coloration remain elusive. Contemporary black EC materials, such as donor-acceptor copolymers[6–8], triphenylamine-based systems[9], and meta-conjugated polymers[10], all exhibit instability under extended exposure to light (including UV), heat, and humidity. Furthermore, the low ionic and electronic conductivity of these black EC materials creates uneven voltage distribution in large-area devices, with higher voltage at the edges and lower voltage at the center. To compensate, excessive electrical overpotentials—voltages beyond the material's stable operating range—are often applied. This accelerates performance degradation and shortens the device's operational lifespan.

Here, we introduced n-doped poly(benzodifurandione) (n-PBDF) as a black EC active layer to address the inherent limitations of current organic black EC materials. Originally processed from dimethyl sulfoxide (DMSO)—a solvent with a high boiling point and low vapor pressure that complicates large-area coating—we instead developed an on-demand water/ethanol-based ink via a co-solvent precipitation method. This enabled the fabrication of uniform, large-area n-PBDF thin films with precise thickness control using ultrasonic spray-coating. The n-PBDF EC electrodes demonstrated deep black coloration, rapid switching speeds, and exceptional electrochemical stability. Durability tests under harsh conditions—continuous exposure to light, heat (65 °C), and humidity (50% RH) for over 1 month—revealed no degradation in switching performance. To showcase practicality, we engineered transmissive-to-black EC windows that achieve ~5% transmittance in the colored state (550 nm) at 190 nm film thickness, with some configurations achieving as low as ~1% at higher thicknesses, while retaining >50% transmittance when bleached. These devices exhibited remarkable cycling stability (<3% contrast loss after 20,000 cycles at 190 nm) and dynamic solar heat gain coefficient modulation (ΔSHGC ≈ 14% at 90 nm), enabling significant HVAC energy savings (estimated 15–55 MJ/m^2 annually for a mid-rise apartment building) in transitional climates.

Results

Scalable fabrication of n-type conducting polymer, n-PBDF, for black EC electrodes

The development of EC materials that enable reversible oxidation/reduction switching between black and transmissive states, along with their associated processing techniques, is important for commercial applications requiring active control over solar radiation transmittance and visual transparency. Figure 1a illustrates the configuration of an electrochromic device (ECD), consisting of a working electrode (WE) responsible for coloration, a counter electrode (CE) maintaining charge balance, and an electrolyte layer positioned between them. To achieve black electrochromism, the WE must provide broad absorption modulation within the visible light spectrum[6,7]. In this study, we focused on n-PBDF as a promising black EC active material. As a notable example of a self-doped n-type conjugated polymer[11], n-PBDF undergoes anodically driven black color switching under reversible oxidation/reduction conditions, where the doped state corresponds to a bleached state, and the dedoped state transitions to a colored (or neutral) state, as shown in Fig. 1b. n-PBDF was prepared by following a previously reported method[12–15]. Due to its rigid polymer backbone, lack of side chains and being charged states, n-PBDF exhibits poor solubility in conventional organic solvents commonly used for printing processes[16]. The strong interaction between DMSO and n-PBDF enables stable dispersion and long-term shelf-life storage; however, its high boiling point (~189 °C) and low vapor pressure (~0.06 kPa), pose significant challenges for high-quality large-area film printing, requiring elevated processing temperatures, prolonged drying times, precise control of drying rate, and optimized substrate wettability. To overcome these limitations, we applied a ternary-solvent-ink formulation to n-PBDF, utilizing a co-solvent precipitation strategy, as illustrated in Fig. 1c. This ink formulation involves a sequential dispersion process: n-PBDF is initially dissolved in the primary polar solvent, DMSO, followed by the stepwise addition of two mutually miscible polar co-solvents—distilled water as the second solvent and ethanol as the third solvent—to adjust the overall solvent polarity and promote a uniform, additive-free colloidal state. The composition ratio was systematically optimized to 1:2:7 (DMSO/water/ethanol) to ensure stable nano-colloidal dispersion without the uncontrolled aggregation common in other polar solvents, thereby eliminating the need for filtration steps (see further discussion in *Methods* section, Supplementary Figs. 1–3, and Supplementary Table 1). This method prioritizes environmentally friendly solvents, enables rapid preparation under ambient air conditions, and facilitates on-demand filter-free fabrication of high-performance inks.

The prepared inks were optimized for thin-film formation using an automatic ultrasonic spray-coating method. The ternary-solvent formulation balanced capillary flow with external and internal Marangoni flows, preventing defects like the coffee-ring effect and ensuring uniform film formation. Maintaining the spray process temperature at 35–45 °C was critical to preserve this flow balance, enable uniform spreading without dewetting, and achieve rapid drying (30–50 s), yielding smooth, defect-free films (Supplementary Fig. 4). All processing occurred under ambient conditions, enabling precise thickness control across large-area substrates. Figure 1d shows an atomic force microscopy (AFM) height image of an n-PBDF film on glass, revealing a smooth morphology with a continuous nanofibril-like network structure. Supplementary Figs. 5–6 confirm dense stacking of n-PBDF films on indium tin oxide (ITO) substrates, reducing root-mean-square surface roughness from ~5.8 nm (bare ITO) to 4.0 nm, consistent with SEM data (Supplementary Fig. 7). Figure 1e, f demonstrate uniform deposition of a 32 nm-thick n-PBDF film on a 160 × 160 mm^2 glass substrate, achieving ~1390 S/cm average conductivity with uniform spatial distribution. Notably, n-PBDF films were fabricated at low temperatures without inert-atmosphere post-annealing, demonstrating compatibility with thermally sensitive flexible plastic substrates (Supplementary Table 2). Figure 1g illustrates film thickness tunability through spray cycle adjustments, minimizing structural distortions (e.g., edge-on molecular orientation) in the n-PBDF network (as confirmed by grazing incidence wide-angle X-ray scattering (GIWAXS) measurements with two different doping states in Supplementary Figs. 8–9 and Supplementary Table 3). As expected, electrochemical charge density increased linearly with film thickness.

Electrochromic and electrochemical characteristics of n-PBDF EC electrodes

Figure 2a presents the spectroelectrochemical absorbance spectra for an n-PBDF film electrode across a potential range from −0.3 V to +1.0 V in 0.1 V steps. These measurements, along with all subsequent electrochemical and device analyses, were conducted in a tetrabutylammonium bis(trifluoromethanesulfonyl)imide (TBA-TFSI)-based electrolyte, a system specifically chosen to optimize performance (see details in *Methods* section). As the potential increased, the n-PBDF film underwent electrochemical oxidation, gradually increasing absorbance in the visible and near-infrared regions (NIR-I). Two distinct neutral absorbance peaks at 472 and 860 nm indicated modulation characteristics. Conversely, upon the electrochemical reduction, the film absorbed minimal visible light, indicating a transmissive state. Among the several dominant peaks, we first focused on the $\lambda = 750$ nm region, which exhibited the maximum optical contrast ($\Delta T = T_b - T_c$) in the visible spectrum, allowing us to observe variations in optical properties across colored/bleached (i.e., neutral/doped) states. Generally, electrochemically colored materials follow the Beer-Lambert law, where absorbance increases linearly with the concentration of absorbing species and charge density, proportional to the optical path length or film thickness[4,17]. The n-PBDF EC electrode

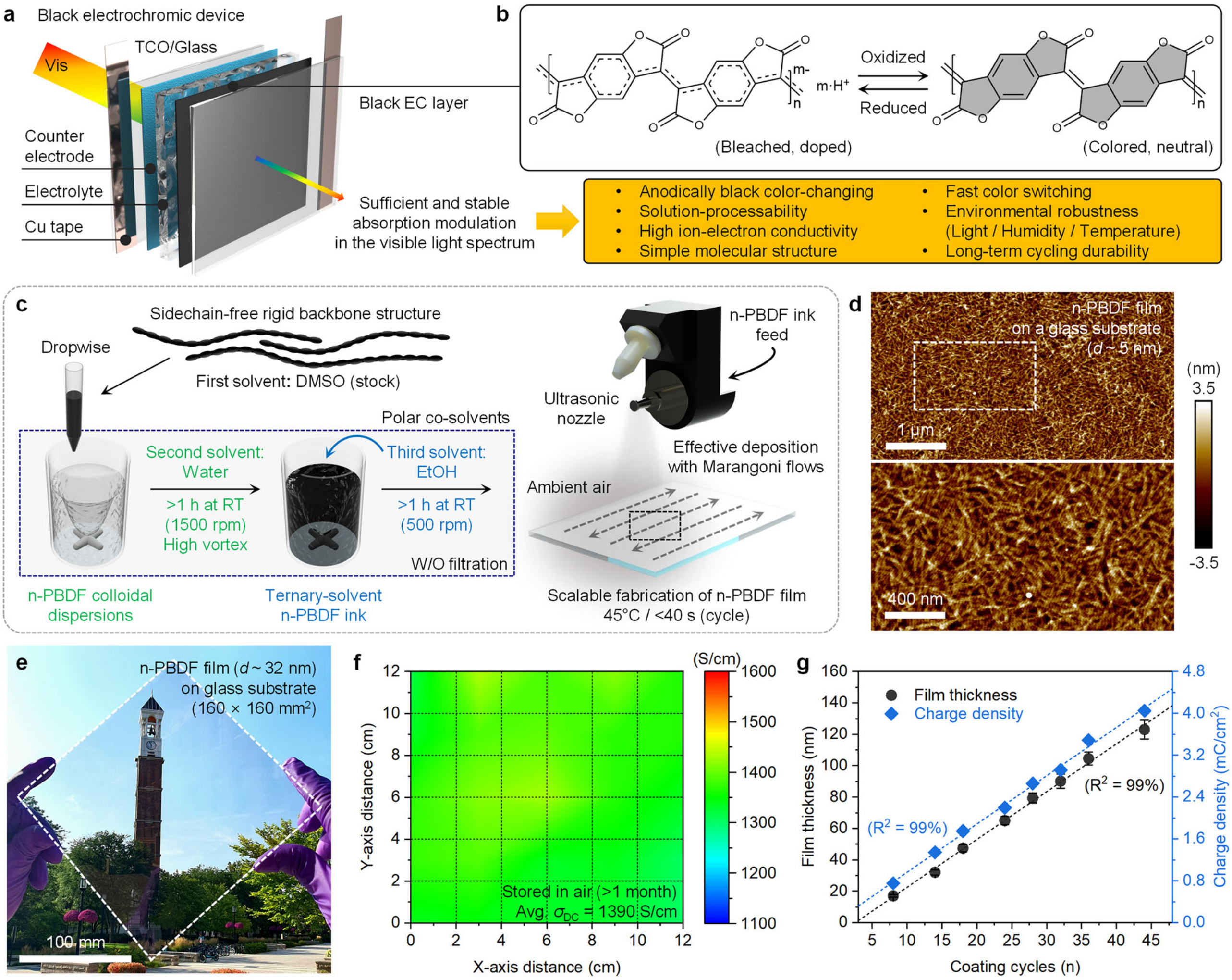

Fig. 1 | Scalable fabrication of n-PBDF ink and films for black EC electrodes. **a** Schematic illustration of n-PBDF-based black electrochromic device. **b** Chemical structural changes during electrochemical reactions: oxidation (colored/neutral) and reduction (bleached/doped) of n-PBDF, and its advantages as a black EC layer. **c** Ternary-solvent-ink-formulation for the enhanced solution-processability of n-PBDF and effective deposition using ultrasonic spray coating (USSC) system for rapid, precise and scalable fabrication of n-PBDF films at low processing temperature, and (**d**) AFM height images of n-PBDF thin film ($d \sim 5$ nm). **e** Photograph of USSC-assisted n-PBDF film ($d \sim 32$ nm) on a glass substrate (160×160 mm²), and (**f**) its corresponding mapping data of the measured film conductivity. **g** Reliable controllability of n-PBDF film thickness (at least 12 points from more than three different batches) according to the number of coating cycles, and linear evolution of the charge densities of the correspondent EC electrode layers.

also exhibited a linear increase in absorbance with respect to the charge density (Fig. 2b). According to Beer's law, transmittance decreases exponentially with increasing thickness, with the respective absorption coefficients determining overall attenuation. The optical contrast can be estimated by plotting the transmittance as a function of the film thickness using these corresponding coefficients (Fig. 2c and Supplementary Note 1). The absorption coefficient (α_c) for coloration of n-PBDF was found to be 5.2×10^5 cm^{-1}, approximately an order of magnitude higher than that in the bleached state ($\alpha_b \approx 5.2 \times 10^4$ cm^{-1}). A maximum optical contrast of 69% for the 750 nm wavelength was achieved with a 49 nm thick film. Furthermore, determining the absorption coefficients in colored/bleached states allows for the precise calculation of the optical electrode thickness required to achieve targeted transmittance values. A comprehensive colorimetric analysis of the bleached and colored states of n-PBDF was conducted using the CIE $L^*a^*b^*$ color model (Supplementary Note 1), where L^* represents lightness (0 for black to 100 for white), and a^* and b^* correspond to green-red and blue-yellow color axes, respectively. As human vision has inherent limitations in distinguishing subtle color variations, the chroma (C^*) value serves as an objective metric of color neutrality, with a C^* value below 10 indicating that the color appears neutral gray. Precise thickness control of uniform n-PBDF films broadens the achievable brightness range, expanding lightness modulation (Fig. 2d). While the color difference (ΔE^*_{ab}) increased proportionally with film thickness, the chroma values in the colored state remained below 5, ensuring excellent color neutrality with minimal variation in a^* and b^* (Fig. 2e).

The intrinsic electrochemical kinetic behavior of n-PBDF EC electrodes directly influences overall color-switching performance and coloration/bleaching efficiency (CE/BE), as shown in Fig. 2f. Understanding the charge transport/storage mechanisms of n-PBDF EC electrodes is required to achieve high-performance black EC applications. The spectroelectrochemical kinetics of n-PBDF films with four different thicknesses were measured (Supplementary Fig. 11), and CE and BE were determined using the slope of curves corresponding to 95% optical contrast ($\lambda = 750$ nm) at the applied charge density (Supplementary Fig. 12)[4]. The average BE value (606 cm²/C) was higher than the average CE value (517 cm²/C), indicating that the bleaching process is more energy-efficient than the coloring process. Furthermore, the coloration/bleaching switching time (t_c & t_b) (based on 95% optical

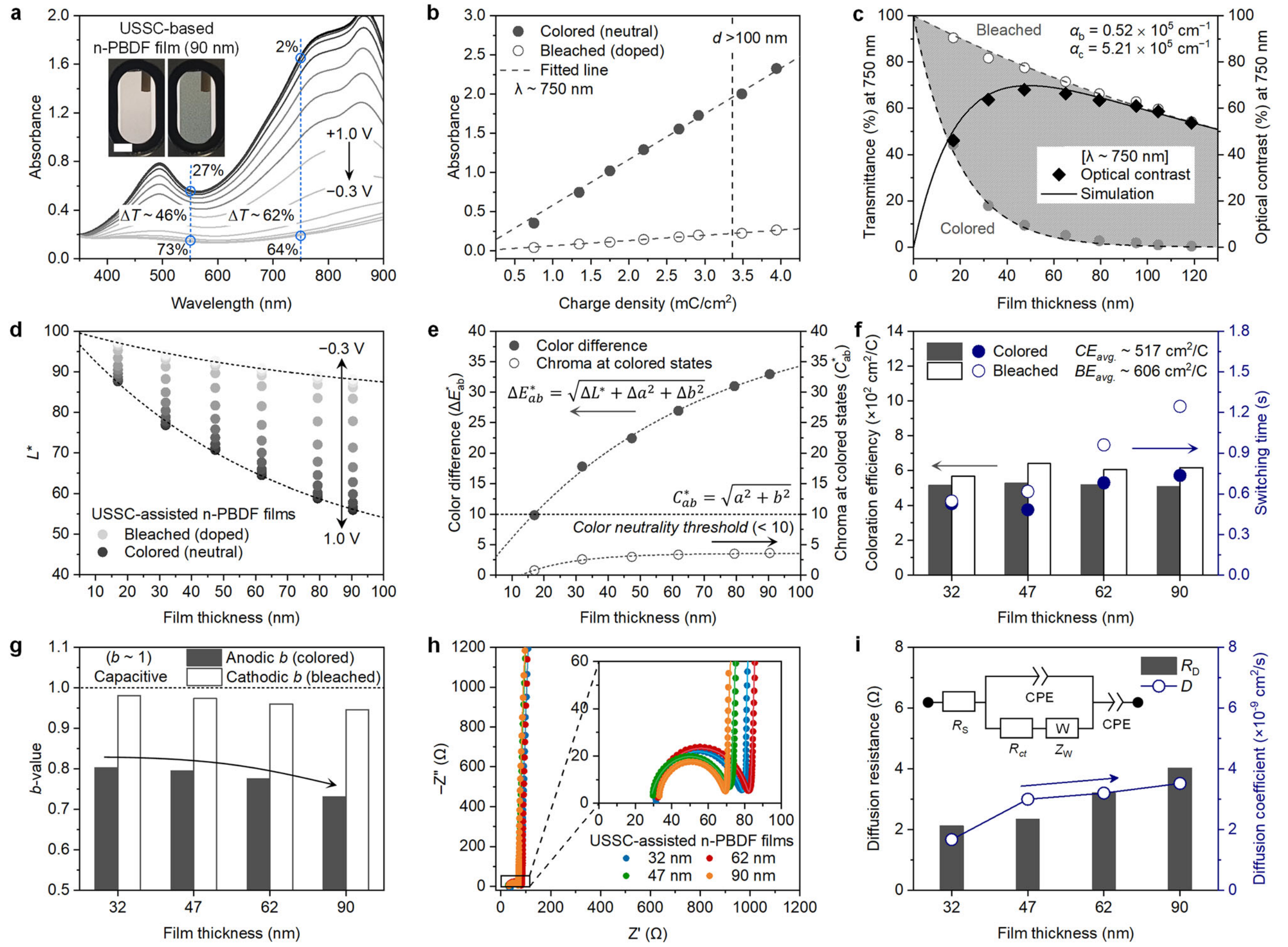

Fig. 2 | Electrochromic and electrochemical performances of n-PBDF EC electrodes. a Spectroelectrochemical analysis of n-PBDF film electrode (d ~ 90 nm) across an applied potential of −0.3 V to +1.0 V vs. Ag/AgCl (with 0.1 V step) (inset: photo images of the EC electrode, scale bar: 4 mm). **b** Progression of absorbance (i.e., optical density) in colored/bleached states of various n-PBDF films against charge density. **c** Transmittance and optical contrast (derived from exponential decay subtraction at colored and bleached states) of films as a function of thickness, measured at $\lambda = 750$ nm. Scatter plot of lightness (**d**) and color difference and chroma for colored states of n-PBDF films (**e**), both as functions of thickness, based on CIE $L^*a^*b^*$ color coordinate. **f** Composite coloration efficiencies and switching times for n-PBDF films across four different film thicknesses, calculated at a 95% optical contrast change at $\lambda = 750$ nm. **g** b values of the n-PBDF films, derived from anodic and cathodic peak current ratios in cyclic voltammograms (scan rates from 2 to 100 mV s^{-1}). **h** Overlay of Nyquist plots of n-PBDF films from EIS measurement in the frequency range of 100 kHz to 0.1 Hz with fitting (inset: high frequency region). **i** Parameters analyzed from the fitted Nyquist plots using an equivalent circuit model (inset): diffusion resistance and diffusion coefficients.

contrast) demonstrated a swift switching response, ranging from 0.5 to 1.3 s. As the electrode thickness increased, the t_b gradually became longer than the t_c. This kinetic asymmetry is attributed to the decoupling of rapid interfacial charge transfer from the slower, diffusion-limited bulk structural relaxation that governs the overall optical switching time[14,18–20]. To analyze the kinetic behavior of n-PBDF EC electrodes, cyclic voltammograms (CV) were recorded at different potential sweep rates (2–100 mV s^{-1}); based on these measurements, the b value and charge storage contributions were analyzed (Supplementary Note 2 and Supplementary Fig. 13). The b value[21], defined as the slope of anodic and cathodic current peaks with respect to the sweep rate (Supplementary Fig. 14 and Supplementary Table 4), provides insight into charge storage mechanisms with the distinct values for each process highlighting an inherent CV asymmetry (Fig. 2g). The cathodic b value averaged 0.96 (b ~ 1; capacitive, b ~ 0.5; diffusive), indicating a rapid capacitive charge storage regime with peak current scaling linearly to the sweep rate, enabling immediate charge injection at the electrode/electrolyte interface and supporting a linear bleaching process. This behavior reflects a gradual "disorder-to-order" structural relaxation during the bleaching process[14,20]. In contrast, the anodic process, corresponding to an "order-to-disorder" transition, included a slower faradaic process due to additional redox reactions requiring an energy barrier to disrupt the ordered polymer structure, lowering to ~0.78 on average ($0.5 < b < 1$: transition region between capacitive and diffusive). As the film thickness increased, the overall b value gradually decreased, reflecting an increasing faradaic contribution during color switching. Next, Dunn's method[21] was employed to investigate the charge storage characteristics of n-PBDF EC electrodes by quantitatively assessing the contributions of surface-capacitive and diffusion-controlled mechanisms (Supplementary Note 2). At low scan rates, both control mechanisms coexisted, confirming the pseudocapacitive behavior of the n-PBDF electrode. The predominant charge storage regime was the fast surface-controlled reaction, with a minor contribution from diffusion. Additionally, as the electrode thickness increased, the influence of the slow diffusion-controlled regime gradually became more significant, affecting the switching response (vide supra) (Supplementary Figs. 15–17).

Electrochemical impedance spectroscopy (EIS) was conducted to investigate the diffusion characteristics of n-PBDF film electrodes with varying thicknesses (Fig. 2h, i). Measurements were performed at ~0.34 V (i.e., open-circuit voltage) versus an Ag/AgCl reference electrode across a frequency range of 100 kHz to 0.1 Hz. Nyquist plots displayed semicircles at high frequency, extending vertically towards low frequencies revealing typical capacitive behavior (Fig. 2h)[22]. EIS fitting using an equivalent circuit (inset of Fig. 2h, i) showed a stable charge transport pathway, with an average charge transfer resistance (R_{CT}) of 47 ohms and a uniform semicircle distribution across thickness variations (Supplementary Note 2 and Supplementary Table 5). Finite-length Warburg diffusion analysis indicated a gradual increase in diffusional resistance (R_{D}) with thickness due to extended ion diffusion pathways, which could delay the switching speed. The diffusion coefficient (D^*) increased, indicating the formation of additional ion transport pathways and a change in crystallite size. This is supported by GIWAXS measurements showing a decrease in the crystal coherence length (L_{c})[23] for the π-π stacking (010) and lamellar-stacking (100) peaks with increasing film thickness from ~40 to 100 nm (Supplementary Fig. 9 and Supplementary Table 3). This reduction in long-range order signifies an increase in structural disorder, which provides the primary pathways for ion transport in mixed-conducting polymers[24,25]. Therefore, the expansion of these ion-conductive disordered regions and the associated increase in porosity of the nanofibrous network (Fig. 1d and Supplementary Figs. 5–6) create more pathways for ion migration, thus enhancing D^*. The concurrent decrease in b value suggests an increasing contribution of Faradaic processes in thicker films, where charge transport shifts from a predominantly capacitive mechanism to one progressively influenced by ion diffusion. In particular, as the size of the ordered regions decreases in thicker films, changes in the polymer microstructure may influence the ion transport pathways, further affecting the electrochemical behavior of n-PBDF-based EC electrodes.

Weathering robustness of n-PBDF EC electrodes

Organic EC materials offer distinct advantages, including diverse functionalities and color options, excellent processability, and rapid response times, underscoring their potential as next-generation applications. However, low stability and durability, particularly under ambient outdoor conditions, remain a bottleneck to their practical application and commercialization[1–4]. In particular, EC windows, inevitably exposed to outdoor weather conditions, must address three primary environmental factors that frequently arise unpredictably and simultaneously, significantly affecting the stability and durability of organic EC materials: (1) solar radiation including UV light, (2) thermal stress induced by radiative heat or elevated ambient temperatures, and (3) humidity associated with moisture and oxygen. Although extensive research has investigated the instability of organic EC electrodes under each of these conditions individually[4,10,26,27], practical implementation necessitates the integrated assessment of all three factors. To enable the viable fabrication of organic EC windows, it is essential to investigate and achieve intrinsic environmental stability and durability in organic EC electrodes alone, independent of encapsulation or assembled device configurations, when exposed to harsh weathering conditions. In exploring the inherent durability of n-PBDF EC electrodes, we subjected as-prepared and unencapsulated films ($d \approx 90$ nm and 150 nm) to an accelerated weathering test in a Q-SUN Xe-3 chamber (Q-Lab, USA) for over 1 month (see *Methods* section for details). The test followed ISO 11341 (or ISO 16474-1:2013) protocols, commonly applied to exterior paints and varnish coatings, with conditions set at 1000 W/m^2 (cf. 0.51 W/m^2/nm at 340 nm), irradiance from xenon lamps, 50% relative humidity (RH), and a chamber temperature of 65 °C[28]. The films were oriented directly toward the lamps for full light exposure and evaluated at specific intervals of 24, 48, 96, 192, 384, and 768 h (1, 2, 4, 8, 16, and >32 days), as shown in Fig. 3a.

We investigated the impact of weathering exposure on n-PBDF EC electrodes using UV-Vis-NIR absorbance spectroscopy (350–1800 nm), with results presented in Fig. 3b, d. Measurements were performed on n-PBDF EC electrode films directly exposed to weathering conditions, tracking temporal changes in the absorbance spectra with data averaged from at least three measurements, as reflected by error bars showing small deviations. Over 768 h of weathering exposure, a modest increase in neutral peak absorbance occurred in the visible range, while a gradual decline in absorbance was observed in the NIR polaron region. These changes suggested evolving optical properties in the film, driven by reduced self-doping interactions in n-PBDF under prolonged stress[14]. To complement these observations, attenuated total reflectance Fourier-transform infrared spectroscopy (ATR-FTIR) was performed on the same weathered samples to investigate chemical structural changes and associated bond cleavages, with spectra detailed in Supplementary Fig. 18[29]. No significant structural degradation was observed from 24 to over 768 h (>32 days) of exposure, confirming the chemical and structural stability of the material. Notably, the C=O stretching peak of five-membered lactone moieties, initially observed at 1780 cm^{-1} as a fingerprint of n-PBDF, exhibited a marginal blueshift to higher wavenumbers with increasing weathering exposure time. This shift indicates a strengthened C=O bond due to an enhanced electron-withdrawing effect and a minor reduction in doping interactions between the C=O group and protons. Conversely, the C=C bonding peak at 1450 cm^{-1} showed a significant redshift, indicating increased localization of the C=C bond in the resonance structure, which enhanced its double-bond character and indicated partial dedoping with prolonged environmental exposure. These ATR-FTIR trends align with the reduction in the NIR polaron region, collectively illustrating the gradual chemical and doping-related changes in n-PBDF under extended environmental exposure.

Furthermore, EC kinetic cycling tests were performed 50 times for each sample at distinct wavelengths ($d \sim 90$ nm at $\lambda = 750$ nm, $d \sim 150$ nm at $\lambda = 550$ nm) (Fig. 3c, e). Remarkably, even after >768 h of continuous exposure, the reduction in optical contrast was minimal (less than 2%), fully satisfying the weathering stability requirements for outdoor EC applications. Although partial dedoping of the n-PBDF EC electrodes occurred due to exposure to light, heat, and moisture during accelerated weathering, the electrodes demonstrated excellent photostability, robust resistance to temperature and humidity, negligible structural degradation, and strong electrochemical resilience. These properties were attributed to two key factors: the unique structural features of n-PBDF, characterized by the absence of side chains and robust interchain stacking of its extended planar conjugated backbones, and its capacity to sustain doping levels under varying moisture and drying conditions[12–14]. The n-PBDF EC electrode, exhibiting excellent weathering robustness, provides a critical foundation for enhancing the stability of EC windows against external environmental factors, such as water vapor, oxygen, light, and heat, as demonstrated by preliminary tests on dry films under harsh conditions without encapsulation. This inherent robustness not only facilitates easier handling but also highlights the material's intrinsic stability as a key factor for potentially reliable EC devices, with effective encapsulation and suitable electrolyte mixtures likely to further enhance its performance during fabrication.

Fast switching and durable anodic-color-changing black electrochromic devices

Figure 4a illustrates the components of a transmissive-to-black switching EC device built with an n-PBDF EC electrode. The device consists of an EC layer (i.e., WE) made of a single n-PBDF film and a transparent ion storage layer (i.e., CE) consisting of mesoporous ITO nanoparticles (m-ITO). These electrodes face each other, separated by a UV-curable solid-state electrolyte layer containing the aforementioned bulky ionic electrolyte system (TBA-TFSI). The m-ITO layer, prepared from a dispersion solution of ITO nanoparticles using the same ultrasonic spray-coating technique, allows precise charge density control, measured as mass loading density (mg cm^{-2}) instead of thickness. This method yields a stable electrical double-layer capacitance layer with minimal color change under varying applied

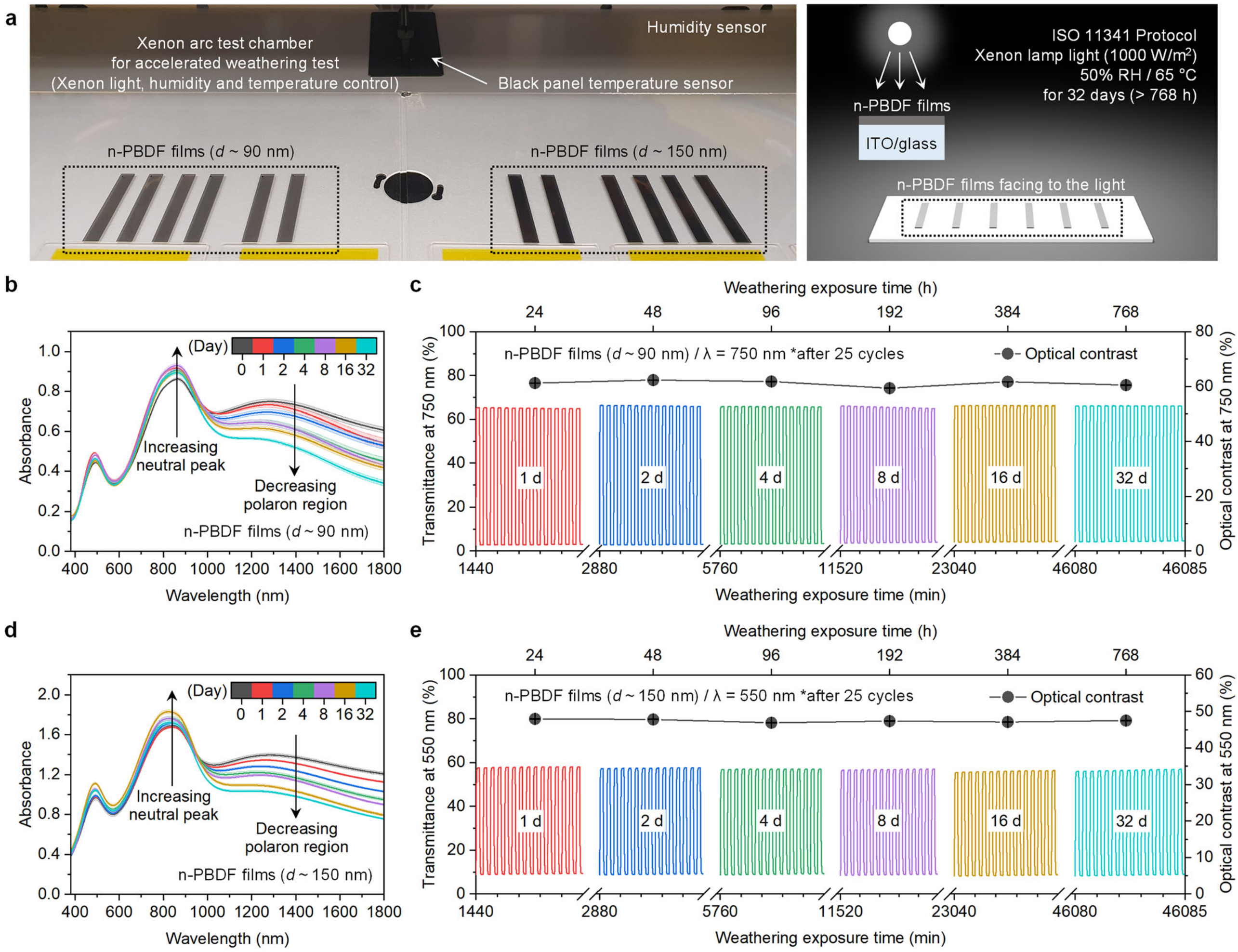

Fig. 3 | Environmental robustness of n-PBDF EC electrodes under weathering conditions. a Interior view of the accelerated weathering test chamber, showing 12 samples coated with USSC-assisted n-PBDF films of two different thicknesses (d ~ 90 and 150 nm), positioned facing toward a Xenon lamp light without additional surface encapsulation. Accelerated weathering tests were conducted continuously for >768 h (32 days) under 1000 W/m² light intensity, 50% RH, and a chamber temperature of 65 °C. **b** UV-Vis-NIR absorbance spectra ($\lambda = 350$–1800 nm) of 90 nm n-PBDF films, analyzed to track changes in absorbance peaks immediately after weathering exposure (day 0 samples exposed to ambient conditions for the same duration) (measured at least 3 points for each exposed sample). **c** Operational cycling stability tests for electrochemical switching behavior of 90 nm n-PBDF films at $\lambda = 750$ nm, evaluating weathering robustness and electrochemical durability. **d** UV-Vis-NIR absorbance spectra of 150 nm n-PBDF films, consistent with (**b**), performed after weathering exposure (measured at least 3 points for each exposed sample). **e** Electrochemical stability tests of 150 nm n-PBDF films at $\lambda = 550$ nm, conducted under conditions identical to those in (**c**).

potentials (Supplementary Figs. 19–23), offering a charge capacity substantially higher than that of conventional flat ITO due to its mesoporous structure, thereby ensuring effective charge balance with the n-PBDF WE layer within the device[30]. To accommodate the target film thickness of n-PBDF and ensure balance with a broader charge capacity, a CE layer with increased mass loading density of the m-ITO layer was prepared, and the corresponding EC device was fabricated. Using this architecture, EC devices were fabricated by selectively adjusting the thickness of the n-PBDF active layer, followed by spectroelectrochemical analysis and evaluation of electrochemical switching stability. The overall transmittance in the visible region was modulated by increasing the applied potential from −1.0 V to +1.8 V. For a 90-nm-thick n-PBDF WE, an optical contrast exceeding 65% was achieved at 750 nm (4% colored state to 69% bleached state) (Fig. 4b). Subsequently, 550 nm, at which the human eye is most sensitive, was adopted as a reference for achieving a vivid and deep black coloration. As previously discussed in Fig. 2b, c, optical simulations were performed by fitting the exponential decay of colored and bleached transmittance at 550 nm as a function of n-PBDF film thickness. The absorption coefficient for the bleached state (α_b) was determined to be 3.7×10^4 cm^{-1}, significantly lower (approximately fivefold) than that for the colored state ($\alpha_c = 1.6 \times 10^5$ cm^{-1}) (Supplementary Fig. 24). Based on these calculated coefficients, a minimum n-PBDF WE thickness of 290 nm was found to be necessary to achieve a transmittance below 2% at $\lambda = 550$ nm. Consequently, a deep black coloration was realized, exhibiting an optical contrast of 41% and a minimum transmittance of 1.8% at $\lambda = 550$ nm (Fig. 4b).

In Fig. 4c, the CIE $L^*a^*b^*$ color coordinates demonstrated a significant brightness difference between the bleached and colored states, with L^* values of 90 and 14, respectively. The projections of a^* and b^* remained near zero, while the C^* value stayed below 10, confirming color neutrality without intermediate hues. This feature makes the ECDs suitable for applications such as dimmable windows, where precise modulation of intermediate shades is required[7]. Both devices showed robust cycling stability, with performance degradation averaging less than 4% after 1000 cycles. The 90-nm n-PBDF-based ECD (Fig. 4d) showed rapid switching, with coloration and bleaching times (t_c and t_b) of 0.37 s and 0.43 s, respectively. In Fig. 4e, BE and CE values of 554 and 519 cm²/C, reflecting optical density (OD) variations consistent with the previously observed kinetic behavior. During the coloration (dedoping) process, it shows a nonlinear OD response under the influence of strong neutral peaks at 490 nm and 860 nm

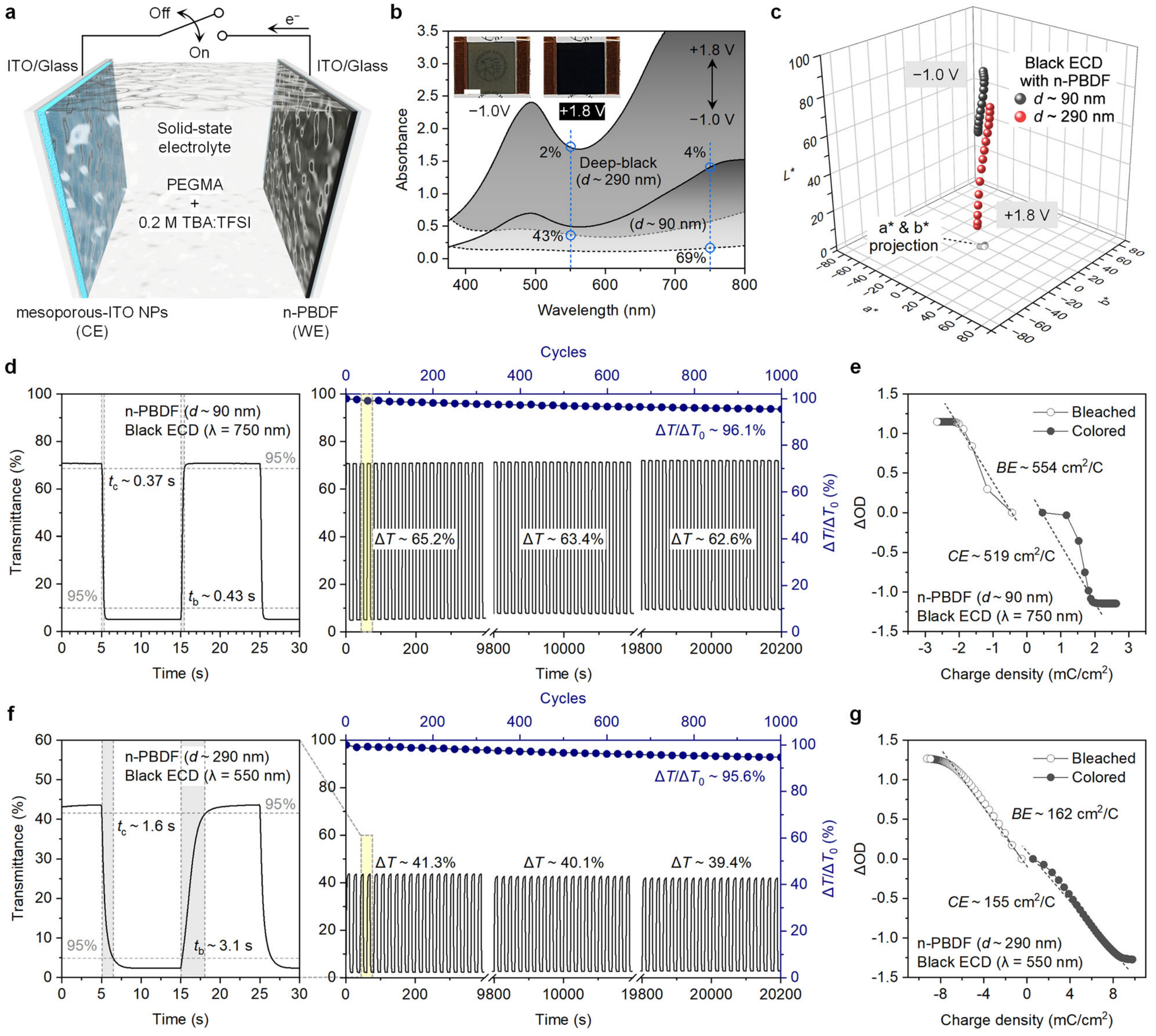

Fig. 4 | Characterizations of fast switching and durable n-PBDF-based deep black ECD. a Schematic of n-PBDF-based black electrochromic devices (ECD), incorporating a mesoporous ITO nanoparticle layer as an ion-storage layer. Solid-state electrolyte layer is photo-crosslinked between the facing two electrodes during the ECD assembly. **b** Spectroelectrochemical analysis of black ECDs fabricated with two different film thicknesses (inset: photo images of ECD showing a deep black coloration with a 290 nm n-PBDF working electrode, scale bar: 8 mm). **c** 3D plot of CIE $L^*a^*b^*$ coordinate distribution of black ECDs based on 90 and 290 nm n-PBDF films (depicted with plane projections of a* and b*). Investigation of **d** kinetic switching speeds and electrochemical cycling stability for a 90 nm n-PBDF black ECD, including changes in optical contrast, and **e** coloration and bleaching efficiency at $\lambda = 750$ nm, reflecting 95% optical contrast. Similar investigation for a 290 nm n-PBDF deep black ECD, focusing on **f** switching speed and the cycling stability, including changes in optical contrast, with **g** coloration and bleaching efficiency measured at $\lambda = 550$ nm.

(Supplementary Fig. 10), indicating structural transitions from n-PBDF to PBDF[14]. By contrast, the ECD with a 290-nm n-PBDF film (Fig. 4f and Supplementary Movie 1) recorded $t_c = 1.6$ s and $t_b = 3.1$ s at 550 nm, respectively. This longer bleaching time correlates with increased electrode thickness, as observed in Fig. 2f. Meanwhile, Fig. 4g shows BE and CE values of 162 and 155 cm^2/C at 550 nm, where OD changes during bleaching and coloration remain linear, ensuring predictable modulation with color neutrality for visual/privacy applications.

Large area transmissive-to-black electrochromic windows

In addition to the rapid and robust EC performance demonstrated earlier, the scalability of n-PBDF EC electrodes for large-area applications must be considered for the practical implementation of EC windows. As shown in Fig. 1e, the ternary-solvent-based n-PBDF ink and precise spray process control enabled the fabrication of uniform large-area n-PBDF black EC electrodes ($d \sim 190$ nm, $T \sim 5\%$ at 550 nm) without size or thickness constraints, allowing the successful fabrication of an 80 × 60 mm^2 EC window (Fig. 5a and Supplementary Movie 2). Owing to the high electron-ion conductivity of the n-PBDF, negligible differences (switching time gap $\Delta t < 0.2$ s) in switching speeds between the center ($t_b = 1.76$ s, $t_c = 1.51$ s) and edges ($t_b = 1.91$ s, $t_c = 1.32$ s) of the large-area EC window were observed (Fig. 5b). Furthermore, in Supplementary Fig. 25, the electrode exhibited uniform black coloration across its entire area, maintaining color neutrality within the same voltage range while achieving a significant brightness change ($\Delta L^* \approx 60$) and fast switching speeds. Notably, even after up to 20,000 cycles in a cycling test, the average optical contrast of 44% showed a loss of less than 3% (optical decay ratio <7%), demonstrating exceptional stability among reported EC windows. Additionally, the low processing temperature enables highly uniform and precise coatings on thermally

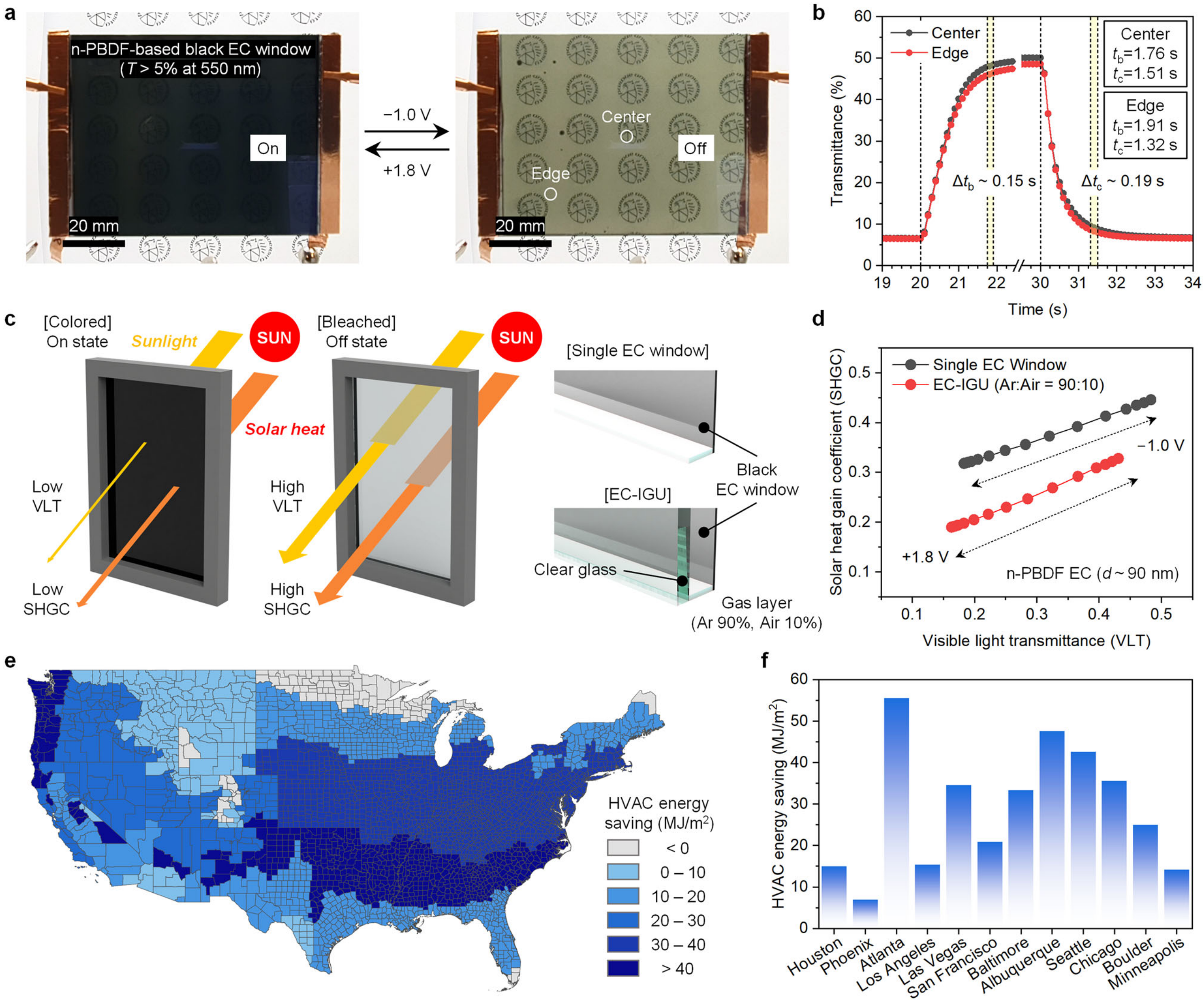

Fig. 5 | Large-area transmissive-to-black n-PBDF-based EC windows and building energy simulation. a Photographs of an n-PBDF-based black EC window (80×60 mm^2) featuring an n-PBDF film ($d \sim 190$ nm, achieving $T \sim 5\%$ at 550 nm) under applied potentials of +1.8 V (left) for the colored state and −1.0 V (right) for the bleached state and. **b** Optical transmittance at $\lambda = 550$ nm with on/off switching duration of 10 s, measured at the center (black) and edge (red) regions of the black EC window in (**a**). **c** Schematic illustration of a large-area n-PBDF-based black EC windows designed for active modulation of solar light and heat, accompanied by cross-sectional views of a single EC window and an EC insulating glass unit (EC-IGU). **d** Distribution of solar heat gain coefficient versus visible light transmittance for a single n-PBDF ($d \sim 90$ nm) EC window and an EC-IGU window, evaluated by applied potentials. **e** Simulated HVAC energy savings map for a midrise apartment building across the United States, incorporating n-PBDF-based EC window (with EC-IGU window). **f** Estimated annual HVAC energy savings for a midrise apartment building in representative U.S. cities.

sensitive flexible plastic substrates, such as PET, facilitating the large-scale fabrication (140×140 mm^2) of flexible black EC devices (Supplementary Fig. 26). These results highlight the promising potential of n-PBDF EC electrodes for large-scale black EC applications, not only in planar configurations but also on curved or contoured three-dimensional surfaces.

Black EC windows serve as functional building fenestration, enabling not only modulation of visible light but also effective and active management of solar energy across the full spectrum (Fig. 5c). To investigate this performance, two configurations were simulated: a single n-PBDF-based EC window and an EC-insulated glazing unit (EC-IGU) incorporating an argon gas layer (Supplementary Fig. 28). Building on this design, energy efficiency and active modulation are critical for optimizing black EC window performance, requiring high optical contrast with a high transmittance at the bleached state alongside color neutrality. To meet these demands, a 90-nm n-PBDF electrode, selected from various thicknesses, was utilized in this study. The capabilities of the n-PBDF-based EC window were quantified using spectroscopic measurements with an integrating sphere under ambient background conditions (Supplementary Fig. 27). These measurements enabled the calculation of the solar heat gain coefficient (SHGC) to assess the thermal regulation performance of n-PBDF EC windows in building applications (Supplementary Note 3). Results in Fig. 5d showed that the EC-IGU, owing to enhanced insulation, achieves a lower SHGC range than the single n-PBDF EC window, with a maximum SHGC modulation (ΔSHGC) of 0.14 (14%) for both systems (Supplementary Table 6), with comparable visible light transmittance (VLT) modulation. This demonstrates that effective SHGC modulation, achievable with both single and IGU configurations, supports the broad applicability of n-PBDF EC windows across diverse regional and climatic conditions.

To evaluate the HVAC energy-saving performance of n-PBDF EC windows installed in the standard windows of midrise apartments constructed since 1980, building energy simulation software (EnergyPlus) was employed (Supplementary Note 3 and Supplementary Fig. 29). The annual total energy savings of HVAC systems across representative U.S. cities spanning diverse climate zones are depicted in a distribution map in Fig. 5e. The results revealed substantial HVAC energy savings, particularly in moderate to transitional climate zones where both heating and cooling demands coexist. Notably, major metropolitan and/or coastal cities, such as Atlanta, Albuquerque, Seattle, Chicago, Baltimore, and San Francisco, achieved annual energy savings ranging of 15–55 MJ/m^2 upon application of n-PBDF EC windows (Fig. 5f). These regions, distinguished by dense clusters of residential and commercial buildings and climatic conditions necessitating both winter heating and summer cooling, fully leverage the heat-shielding and insulating capabilities of EC windows. Moreover, mid-rise and high-rise buildings with large window areas are prevalent in moderate climate zones, offering significant potential for enhancing overall building energy efficiency through window retrofitting alone. Given the high concentration of population and buildings in these areas, the widespread implementation of EC windows could significantly contribute to reducing national HVAC energy consumption and associated carbon emissions.

Discussion

We have demonstrated that n-PBDF EC electrode stands as a robust organic conductor for high-performance black EC windows, effectively addressing key challenges in performance, durability, and scalability. By integrating a ternary-solvent-ink formulation with Marangoni flow-assisted ultrasonic spray coating, we achieved uniform large-area n-PBDF films under ambient conditions without surfactants or additional processing steps, enabling precise control over film morphology and electrochemical properties for consistent EC performance. Notably, these electrodes demonstrated unprecedented robustness, enduring over 768 h of accelerated weathering conditions (xenon arc lamp light with UV, 65 °C, 50% RH), surpassing longstanding environmental stability limits of organic EC materials. When fabricated into EC devices, they deliver deep black coloration ($T \sim 5\%$ at 550 nm), black coloration with color neutrality, rapid switching speeds, and robust cycling stability (>20,000 cycles), while maintaining consistent performance and scalability for large-area applications. Furthermore, building energy simulations highlighted the practical benefits, revealing a dynamic SHGC modulation of n-PBDF EC windows, which supports significant HVAC energy savings in transitional or mixed climates. By balancing performance, scalability, and durability, these findings position n-PBDF EC electrodes as a compelling alternative to inorganic EC systems, setting a benchmark for organic EC technologies and paving the way for their broader integration into diverse energy-efficient architectural solutions and adaptive visual applications.

Methods

Materials

Pure deionized water (18.2 MΩ cm) was obtained using a Millipore Direct-Q 3 UV water purification system (Merck Millipore). Methanol (MeOH, 99.8%), ethanol (EtOH, anhydrous, 200 proofs, 99.5%), isopropyl alcohol (IPA, 99.5%), and acetone (>99.5%) were purchased from Fisher Scientific (USA). Indium tin oxide nanoparticles (In_2O_3:SnO_2 = 9:1, 99.99%, Blue) were sourced from US Research Nanomaterials, Inc. (USA). Tetrabutylammonium bis(trifluoromethanesulfonyl)imide (TBA-TFSI, >99%), dimethyl sulfoxide (DMSO, anhydrous, 99.9%), propylene carbonate (PC, anhydrous, 99.7%), Tris(4-bromophenyl)ammoniumyl hexachloroantimonate (Magic Blue), acetonitrile (ACN, anhydrous, 99.8%), poly(ethylene glycol) methacrylate (PEGMA, average Mn-360), 2-hydroxy-2-methylpropiophenone (HMP, 97%), (3-glycidyloxypropyl)trimethoxysilane (GLYMO, >98%), and ethylene glycol (EG, anhydrous, 99.8%) were obtained from Sigma-Aldrich. All materials were used as received unless otherwise specified. The n-doped poly(benzodifurandione) (n-PBDF) was synthesized and prepared in DMSO solvent, following a previously reported method[12].

Ternary-solvent conductive ink formulation

A ternary-solvent-based n-PBDF ink was prepared via a co-solvent precipitation method under ambient temperature and air conditions, without surfactants or dispersing agents. The synthesized n-PBDF solution in the first solvent, DMSO (with a solute concentration of 5–7 mg/mL), was added dropwise into the second solvent, distilled water, stirred at >1500 rpm to create a vigorous vortex. After 2 h of mixing, the resulting dark n-PBDF polymeric nano-colloids were formed without additional centrifugation or washing for separation or pH adjustment. The third solvent, anhydrous ethanol, was then added to the dispersion and stirred gently at 500 rpm for 30 min to produce the final conductive ink. Beginning with the second solvent, all subsequent solvents, including water and ethanol, were selected as co-solvents that are both water-miscible and polar, allowing flexibility in solvent choice. These solvents—DMSO, water, and ethanol—were combined at an optimal 1:2:7 volume ratio. This specific ratio was systematically optimized to overcome the processing limitations of pure DMSO (e.g., high boiling point, low vapor pressure). By introducing water and ethanol as polar co-solvents, a stable nano-colloidal dispersion of n-PBDF was achieved without significant aggregation, eliminating the need for post-ink filtration, ensuring uniform wetting and coating. The ink concentration was tuned by adjusting the amount of the third solvent, chosen for its low surface energy and boiling point (e.g., ethanol), depending on the coating or printing method. Optionally, low-surface-energy solvents such as 1-butanol or isopropyl alcohol could be added in small amounts to enhance surface wettability.

Preparation of redox-active n-PBDF film electrodes

Substrates, including slide glasses (Corning Inc., USA), ITO-coated glasses (>15 ohm/sq.), and Si wafers (University Wafer, n-type, SSP, prime, USA), were cleaned by consecutive sonication in deionized water, acetone, and isopropanol for 15 min each. After drying with compressed nitrogen, the substrates underwent UV-ozone treatment (Jelight XX-140, Ultraviolet-Ozone Cleaner) for 20 min to eliminate organic residues and enhance the wettability of the conductive polymer ink. An automated ultrasonic spray coating system (Sono-Tek, USA) with a 120 kHz ultrasonic nozzle (Impact, Sono-Tek, USA) was used to deposit scalable conductive films from ternary-solvent-based n-PBDF ink. Prior to coating, the ink was stirred at 500 rpm for 30 min to ensure homogeneity. Spray coating was performed with a 50 mm nozzle-to-substrate distance, nitrogen gas for spray shaping, and a stage temperature of 40 °C, with each cycle lasting less than 40 s to allow sequential drying of the wet layers. Adjustable parameters, such as ink flow rate (0.4–1.0 mL/min), coating speed (50–70 mm/s), and number of cycles, were tailored to achieve desired film properties, including uniform coverage, thickness, and surface morphology.

Preparation of mesoporous metal oxide ion-storage layers

ITO nanoparticles (ITO NPs, 160 mg) were dispersed in IPA (20 mL) using a vortex mixer (Fisher Scientific) under ambient conditions, achieving a stable dispersion up to 8 mg/mL. The mixture was then tip-sonicated (Sonic & Materials, Model 750, USA) at 30% amplitude in an ice bath for 30 min to produce a well-dispersed ink suitable for spray coating. Subsequently, GLYMO surfactant (2 wt% relative to ITO NPs) and EG (1 vol% relative to the entire volume) were added, followed by an additional 30 min of ultrasonication to ensure thorough mixing. The mesoporous ITO (m-ITO) layer was deposited using the same automated spray coating system as described above, with a 50 mm nozzle-to-substrate distance, a flow rate of 0.5–1.0 mL/min, and a coating stage at room temperature to achieve the desired mass loading density (mg/cm^2) at a consistent coating speed of 20 mm/s. The coated substrates were then dried on a hot plate at 120 °C for 20 min to remove residual IPA, preparing them for further analysis and device fabrication.

Thin film characterizations

Sheet resistance was measured using a Filmetrics R50-4PP system equipped with automated mapping capabilities. Film thickness and surface morphology were characterized via atomic force microscopy (AFM) using a Bruker iCON Dimension in tapping mode to enable non-destructive topography analysis. For films exceeding 30 nm in thickness, a surface profilometer (DektakXT, Bruker) was employed. Thickness measurements were performed at a minimum of three distinct points across multiple substrate batches to ensure reliability and reproducibility under consistent processing conditions. UV-Vis-NIR absorption spectra were recorded using an Agilent Cary 5000 spectrophotometer. All characterizations were carried out at room temperature under ambient air conditions. High-resolution images were obtained with a Hitachi S-4800 field emission scanning electron microscope (FE-SEM) operated at 10 kV accelerating voltage and 10 μA beam current.

Electrochemical and electrochromic characterizations of EC film electrodes

Film electrodes were prepared on cleaned ITO/Glass substrates (50 × 7 mm^2) for electrochemical and EC characterizations. Measurements were conducted in a three-electrode cuvette cell equipped with a leakless Ag/AgCl reference electrode (eDAQ Inc.) and a platinum wire CE (diameter: 0.5 mm, >99.99%, metals basis, Thermo Scientific Chemicals). Ferrocene/ferroceniums (Fc/Fc$^+$) were served as an external calibration standard for the reference electrode. The supporting electrolyte was prepared for 0.2 M TBA-TFSI salts dissolved in anhydrous PC solvent, a system well-established for providing a favorable balance between switching kinetics and long-term stability in n-PBDF EC electrodes. The selection of bulky organic ions in electrolyte system is based on previous reports demonstrating their effectiveness in enhancing the long-term operational stability and performance of the electrochemical devices[12,31,32]. Cyclic voltammetry (CV) and electrochemical impedance spectroscopy (EIS) measurements were performed using a VSP multichannel potentiostat (BioLogic Inc.) and analyzed with EC-Lab software. The film electrodes were conditioned via CV cycling for at least three cycles until stable CV profiles were achieved. Spectroelectrochemical spectra of the thin films were recorded in a quartz cuvette by coupling a Cary 5000 UV-Vis-NIR spectrometer (Agilent Inc.) paired with an SP-150 potentiostat (BioLogic Inc.) after post-conditioning. A bare ITO/glass substrate in an identical cuvette filled with the same electrolyte was used to provide an optical baseline of the measurements. Absorbance spectra of the oxidized (colored) and doped (bleached) states were measured at potentials of +1.0 V and −0.3 V, respectively. Switching kinetics of the film electrodes were evaluated via stepwise potential fast chronoamperometry (SPFC) by alternating between oxidizing and reducing potentials for 10 s each, while optical transmittance changes were monitored at a target wavelength over multiple switching cycles. Additional details are provided in Supplementary Note 1 and Note 2.

DLS and Zeta potential measurement

Dynamic light scattering (DLS) measurements of the n-PBDF ink solutions, diluted 100-fold in the second (major) solvent, were carried out using a Wyatt DynaPro NanoStar II (Wyatt Technology, USA). A minimum of 45 μL of solution was loaded into a quartz microcuvette, and measurements were performed at 25 °C with a 120 W air-cooled laser ($\lambda = 662$ nm) and 10 acquisitions per measurement. Zeta potential (ZP) analysis of the same diluted dispersion was carried out using a Malvern Nano-Z instrument (Malvern Ltd., UK), with 0.15 mL of solution placed in a folded capillary cell (DTS 1060, Malvern) and measured using a He-Ne laser ($\lambda = 655$ nm with a maximum power output of 4 mW). For both techniques, each sample was measured three times, and the results were reported as averages with standard deviations.

X-ray scattering measurements

GIWAXS was performed on fully dedoped PBDF samples at Stanford Synchrotron Lightsource (SSRL) beamline 11-3. USSC-assisted n-PBDF thin films ($d \sim 40$ and 100 nm) on 20 × 20 mm^2 Si substrates were prepared at Purdue University, then stored and transported to SSRL under inert atmosphere. The samples were dedoped at the beamline laboratory with 10 mM Magic Blue in ACN solution and rinsed with neat ACN to remove the remaining Magic Blue[14]. The samples were measured under helium atmosphere to maintain an inert environment and to reduce scattering from atmospheric gases at an X-ray energy of 12.7 keV and an incident angle of 0.12°. The sample-to-detector distance was calibrated using a LaB_6 standard and was 301.6 mm. 30 s exposures were taken at three different locations for each film and averaged using the Image J average intensity Z-projection tool.

GIWAXS of as-cast pristine n-doped PBDF samples were measured using a Xenocs Xuess 3.0 instrument with a Cu Kα source (8.04 keV) at an incident angle of 0.12°. The samples were measured under vacuum to reduce scattering from atmospheric gases. The sample-to-detector distance was 120 mm. Two exposures were taken and averaged for each sample.

The GIWAXS patterns were subsequently analyzed using Python with the PyFAI software package[33]. Linecuts were generated by averaging the intensities over a range of angles (χ) and scaled by sin(χ), in-plane linecuts are from 75–90°, and out-of-plane linecuts are from 0–15°. Fitting of the peaks from the linecuts was performed using LMFIT[34] with a pseudo-Voigt peak shape after subtracting a linear background. Coherence lengths (L_c) were then calculated using the Scherer equation: $L_c = 2\pi K/\mathrm{FWHM}$, where K is a shape factor equal to 0.9[35].

Accelerated weathering stability test of n-PBDF films

n-PBDF films with thicknesses of 90 nm and 150 nm were prepared on ITO glass substrates (50 × 7 mm^2) to fabricate n-PBDF EC electrodes without encapsulation or passivation layer, following the previously described method. These samples were transferred into a weathering chamber system (Q-SUN Xe-3, Q-Lab Co., USA) equipped with three 1800 W xenon arc lamps, a daylight-Q filter, and a high-purity water line featuring an additional granular activated carbon filter. The chamber was designed to simulate the AM 1.5G solar spectrum, delivering stable irradiance with a maximum intensity of 1000 W/m^2 (narrow-band control of 0.51 W/m^2/nm at 340 nm). The accelerated weathering stability test was conducted in accordance with the ISO 11341 standard protocol[28]: Varnishes and Paints, Artificial Climate, and Radiation Tests (or ISO 16474-1:2013, ASTM G155). The films were exposed to light for 24, 48, 96, 192, 384, and 768 h (i.e., 1, 2, 4, 8, 16, and 32 days), with the n-PBDF-coated side facing the xenon lamp windows to ensure direct exposure. During testing, the internal temperature in the chamber was actively maintained at 65 °C to compensate for heat generated by the lamps, and the RH was controlled at 50%. A standard sample was exposed to identical conditions to serve as a baseline for further characterizations. Electrochemical kinetic properties and cycling stability measurements (>50 cycles) were performed on the film electrodes retrieved after each exposure duration. Additionally, the absorbance FT-IR spectra of regions not exposed to the electrolyte were measured using a Nicolet 6700 FT-IR spectrometer (Thermo Nicolet Corp.) equipped with an Attenuated Total Reflection (ATR) Smart iTR accessory and a single-bounce diamond crystal. Spectral data were collected over a wavenumber range of 4000–800 cm^{-1}, with a spectral resolution of 4 cm^{-1}, averaging 64 scans. Baseline correction and maximum peak normalization were performed without additional smoothing using OMNIC software (v.8.3, Thermo Nicolet Corp.). The same regions (previously analyzed by FT-IR) were also repeatedly characterized by UV-Vis-NIR absorbance spectroscopy.

Electrochromic device fabrication and characterization

The EC devices were assembled using the prepared n-PBDF films as the WE, ITO NPs (i.e., m-ITO) layer films as the CE, and PEGMA/TBA:TFSI/HMP as the solid-state electrolyte. The ternary-solvent n-PBDF ink and ITO NPs ink dispersion were prepared separately and uniformly coated using an ultrasonic spray coating system, following the previously described method, onto ITO glass substrates ($30 \times 25\,\text{mm}^2$ and $60 \times 80\,\text{mm}^2$). The ITO NPs layer, serving as the cathode, was then annealed at 120 °C for 20 min to remove the solvent. The UV-curable solid-state electrolyte was prepared by mixing PEGMA, 0.2 M TBA:TFSI/PC, and HMP (as UV photo-crosslinker) in a volume ratio of 5:5:1, respectively. The prepared electrolyte was drop-cast onto the cathode layer (ITO NPs layer), followed by placing the anode on top of the electrolyte. The device was then irradiated under a UV lamp (SUNUV, 24 W) for 10 min to induce photo cross-linking of PEGMA and HMP. Copper tape was attached to the ends of both electrodes to apply an electrical potential. The fabricated EC devices were characterized using the same electrochemical procedures described earlier, with additional EC properties measured and calculated according to the methods detailed in Supplementary Note 1. To evaluate the long-term operational stability of the EC devices, switching kinetics were monitored for 1000 to over 2000 cycles under oxidation/reduction bias pulses of 10 s each. The optical transmittance spectra were reference to air, including the transmittance loss through the glass, ITO layer, electrolyte, and ion storage layer (i.e., blank device)[10].

To examine the intrinsic optical properties of n-PBDF-based EC windows, n-PBDF-based black EC windows were prepared using the same fabrication process as described earlier. The solar transmittance and reflectance of the EC windows, encompassing all constituent layers including ITO/glass substrates on both sides for the entire device, were measured across the 300–2500 nm range using a Perkin Elmer Lambda 950 UV-Vis-NIR spectrometer equipped with an integrating sphere. Measurements were calibrated in the background transmittance of the ambient atmosphere, with a certified Spectralon diffuse reflectance standard (Perkin Elmer, calibrated, 60 mm, 99%) employed for validation. The integral transmittance and reflectance in the visible range (380–720 nm) and solar spectrum (300–2500 nm) were determined for each applied potential to the EC windows. These optical spectra were then incorporated into insulating glazing unit (IGU) modeling[36,37] to derive the optical metrics of the windows as functional glazing systems, including VLT and SHGC, as detailed in Supplementary Note 3. Subsequently, these metrics were utilized to conduct advanced building energy simulations, such as EnergyPlus, for comprehensive performance evaluation.

Data availability

The authors declare that all the data supporting the findings of this study are available within the main article and in the Supplementary Information. All other data of this study are available from the corresponding author upon request. Source data is provided in this paper. Source data are provided with this paper.

References

1. Gu, C., Jia, A.-B., Zhang, Y.-M. & Zhang, S. X.-A. Emerging electrochromic materials and devices for future displays. *Chem. Rev.* **122**, 14679–14721 (2022).
2. Wang, J. et al. Roadmap for electrochromic smart devices: From materials engineering and architectures design to multifunctional application. *Prog. Mater. Sci.* **153**, 101461 (2025).
3. Wu, S. et al. Applications of thermochromic and electrochromic smart windows: materials to buildings. *Cell Rep. Phys. Sci.* **4**, 101370 (2023).
4. Li, X., Perera, K., He, J., Gumyusenge, A. & Mei, J. Solution-processable electrochromic materials and devices: roadblocks and strategies towards large-scale applications. *J. Mater. Chem. C* **7**, 12761–12789 (2019).
5. Li, B., Dang, J., Zhuang, Q. & Lv, Z. Recent advances in inorganic electrochromic materials from synthesis to applications: critical review on functional chemistry and structure engineering. *Chem. Asian J.* **17**, e202200022 (2022).
6. Beaujuge, P. M., Ellinger, S. & Reynolds, J. R. The donor–acceptor approach allows a black-to-transmissive switching polymeric electrochrome. *Nat. Mater.* **7**, 795–799 (2008).
7. Savagian, L. R. et al. Conjugated polymer blends for high contrast black-to-transmissive electrochromism. *Adv. Opt. Mater.* **6**, 1800594 (2018).
8. Chen, D. et al. High-performance black copolymers enabling full spectrum control in electrochromic devices. *Nat. Commun.* **15**, 8457 (2024).
9. Zhang, Q., Tsai, C.-Y., Li, L.-J. & Liaw, D.-J. Colorless-to-colorful switching electrochromic polyimides with very high contrast ratio. *Nat. Commun.* **10**, 1239 (2019).
10. Wang, Z. et al. Transparent electrochromic polymers with high optical contrast and contrast ratio. *JACS Au* **4**, 2291–2299 (2024).
11. Wang, C., Guo, K., Deng, Y. & Geng, Y. Design strategy for the synthesis of self-doped n-type molecules. *ChemPlusChem*. **89**, e202400286 (2024).
12. Ke, Z. et al. Highly conductive and solution-processable n-doped transparent organic conductor. *J. Am. Chem. Soc.* **145**, 3706–3715 (2023).
13. Tang, H. et al. A solution-processed n-type conducting polymer with ultrahigh conductivity. *Nature* **611**, 271–277 (2022).
14. Ke, Z. et al. Controlled dedoping and redoping of n-doped poly(-benzodifurandione) (n-PBDF). *Adv. Funct. Mater.* **34**, 2400255 (2024).
15. Liu, G. et al. Selenium dioxide catalyzed polymerization of n-doped poly(benzodifurandione) (n-PBDF) and its derivatives. *Angew. Chem., Int. Ed.* **64**, e202418668 (2025).
16. Nguyen-Dang, T. et al. Air-stable perylene diimide trimer material for n-type organic electrochemical transistors. *Adv. Mater.* **36**, 2312254 (2024).
17. Padilla, J., Österholm, A. M., Dyer, A. L. & Reynolds, J. R. Process controlled performance for soluble electrochromic polymers. *Sol. Energy Mater. Sol. Cells* **140**, 54–60 (2015).
18. Xu, T. et al. High-contrast and fast electrochromic switching enabled by plasmonics. *Nat. Commun.* **7**, 10479 (2016).
19. Chen, L. et al. Unveiling dynamics evolution mechanism of electrochromic process in WO_{3-x} film with thickness dependence. *Electrochim. Acta*. **505**, 144958 (2024).
20. Cui, W. et al. Charge transport properties of PBFDO at various doping levels: an electrochemical control and Hall effect characterization study. *J. Phys. Chem. Lett.* **16**, 6393–6401 (2025).
21. Liu, J. et al. Advanced energy storage devices: basic principles, analytical methods, and rational materials Design. *Adv. Sci.* **5**, 1700322 (2018).
22. Laschuk, N. O., Easton, E. B. & Zenkina, O. V. Reducing the resistance for the use of electrochemical impedance spectroscopy analysis in materials chemistry. *RSC Adv.* **11**, 27925–27936 (2021).
23. Rivnay, J., Mannsfeld, S. C. B., Miller, C. E., Salleo, A. & Toney, M. F. Quantitative determination of organic semiconductor microstructure from the molecular to device scale. *Chem. Rev.* **112**, 5488–5519 (2012).
24. Rivnay, J. et al. Structural control of mixed ionic and electronic transport in conducting polymers. *Nat. Commun.* **7**, 11287 (2016).
25. Thomas, E. M., Nguyen, P. H., Jones, S. D., Chabinyc, M. L. & Segalman, R. A. Electronic, ionic, and mixed conduction in polymeric systems. *Annu. Rev. Mater. Res.* **51**, 1–20 (2021).
26. Bulloch, R. H. & Reynolds, J. R. Photostability in dioxyheterocycle electrochromic polymers. *J. Mater. Chem. C.* **4**, 603–610 (2016).

27. Shen, D. E. et al. Enhancement of photostability through side chain tuning in dioxythiophene-based conjugated polymers. *Chem. Mater.* **34**, 1041–1051 (2022).
28. ISO, E. 11341 (2004) Paints and varnishes–artificial weathering and exposure to artificial radiation–exposure to filtered xenon-arc radiation. European Committee for Standardisation, Brussels, Belgium.
29. Li, Q. et al. A highly conductive n-type conjugated polymer synthesized in water. *J. Am. Chem. Soc.* **146**, 15860–15868 (2024).
30. Shen, D. E., Iyer, D. B., Dejneka, A. M., Reynolds, J. R. & Österholm, A. M. Mesoporous ITO electrodes as optically passive counter electrodes for electrochromic devices. *ACS Appl. Opt. Mater.* **1**, 906–914 (2023).
31. Song, I. et al. An n-doped capacitive transparent conductor for all-polymer electrochromic displays. *Nat. Electron.* **7**, 1158–1169 (2024).
32. Wu, X. et al. Improved stability and performance of an n-type depletion mode poly(benzodifurandione) based organic electrochemical transistor via electrolyte selection. *Chem. Mater.* **36**, 8639–8648 (2024).
33. Ashiotis, G. et al. The fast azimuthal integration Python library: pyFAI. *J. Appl. Cryst.* **48**, 510–519 (2015).
34. Newville, M. et al. lmfit/lmfit-py: 1.3.2. *Zenodo* https://doi.org/10.5281/zenodo.12785036 (2024).
35. Rivnay, J., Noriega, R., Kline, R. J., Salleo, A. & Toney, M. F. Quantitative analysis of lattice disorder and crystallite size in organic semiconductor thin films. *Phys. Rev. B.* **84**, 045203 (2011).
36. Strand, M. T. et al. Polymer inhibitors enable >900 cm^2 dynamic windows based on reversible metal electrodeposition with high solar modulation. *Nat. Energy* **6**, 546–554 (2021).
37. Zhang, Y. et al. Color-neutral smart window enabled by gradient reversible alloy deposition. *ACS Energy Lett.* **9**, 4162–4171 (2024).

Acknowledgements

Ambilight Inc., Research Contract #4000187.02. This work was performed in part at the Research Instrument Center (RIC) at James Tarpo Jr. and Margaret Tarpo Department of Chemistry, Purdue University. GIWAXS measurements (University of Colorado) were supported by the Center for SoftPhotoElectroChemical Systems, an Energy Frontier Research Center funded by DOE, Office of Sciences, BES under Award No. DE-SC0023411. Use of the Stanford Synchrotron Radiation Lightsource, SLAC National Accelerator Laboratory, is supported by the U.S. Department of Energy, Office of Science, Office of Basic Energy Sciences under Contract No. DE-AC02-76SF00515. This work was supported in part by the Colorado Shared Instrumentation in Nanofabrication and Characterizations (COSINC): The COSINC-CHR (RRID: SCR_018985), College in Engineering & Applied Science, University of Colorado Boulder.

Author contributions

W.-J.L. and J.M. conceived the project and planned the experiments. W.-J.L. formulated the ink and optimized film processing. W.-J.L. performed the electrical/electrochemical characterizations and fabricated the electrochromic devices. P.M. assisted in analyzing electrochemistry data with fitting. J.R.T. and M.F.T. performed GIWAXS characterization. Y.T., X.L., and X.R. evaluated solar energy regulation of windows and conducted EnergyPlus simulations. S.S. and W.-J.L. characterized the properties of printable ink dispersions. L.Y. synthesized the bare n-PBDF polymers. I.S. recorded HR-SEM images. W.-J.L. and J.M. drafted the manuscript, and all authors contributed to writing the paper and providing feedback on the manuscript.

Competing interests

J.M. is a co-founder of Ambilight Inc., which financially sponsors this study under a research agreement. He is also a founder of PBDF LLC, focusing on the commercialization of n-PBDF. The other authors declare no competing interests.

Additional information

Supplementary information The online version contains supplementary material available at https://doi.org/10.1038/s41467-025-67271-w.

Correspondence and requests for materials should be addressed to Jianguo Mei.

Peer review information *Nature Communications* thanks Po-Chun Hsu, Jian-Wei Liu, and the other, anonymous, reviewer(s) for their contribution to the peer review of this work. A peer review file is available.